

Article

Plasma-Initiated Grafting of Bioactive Peptide onto Nano-CuO/Tencel Membrane

Tzer-Liang Hu ¹, Guan-Yu Chen ², Shih-Chen Shi ^{3,*}  and Jason Hsiao Chun Yang ^{2,*} ¹ Division of General Neurosurgery, Jen-Ai Hospital, Taichung 41265, Taiwan² Department of Fiber and Composite Materials, Feng Chia University, Taichung 40724, Taiwan³ Department of Mechanical Engineering, National Cheng Kung University, Tainan 70101, Taiwan

* Correspondence: scshi@mail.ncku.edu.tw (S.-C.S.); jasonhcyang@mail.fcu.edu.tw (J.H.C.Y.)

Abstract: A bioactive peptide has been successfully grafted onto nano-CuO impregnated Tencel membranes by a simple and rapid method involving a series of textile processes, and an atmospheric argon plasma treatment that requires no additional solvent or emulsifier. Surface morphology shows an apparent change from smooth, slightly roughened, and stripped with increasing plasma treatment time. The FT-IR characteristic peaks confirm the presence of the CuO nanoparticle and peptide on the extremely hydrophilic Tencel membranes that exhibit a zero-degree contact angle. Prepared nano-CuO/Tencel membranes with 90 s plasma treatment time exhibit excellent antimicrobial activity against *E. coli* and *S. aureus*, and promote fibroblast cell viability with the assistance of a grafted bioactive peptide layer on the membrane surface.

Keywords: Tencel; copper oxide; bioactive peptide; antimicrobial; atmospheric pressure plasma processing



Citation: Hu, T.-L.; Chen, G.-Y.; Shi, S.-C.; Yang, J.H.C. Plasma-Initiated Grafting of Bioactive Peptide onto Nano-CuO/Tencel Membrane. *Polymers* **2022**, *14*, 4497. <https://doi.org/10.3390/polym14214497>

Academic Editor: Francesco Trotta

Received: 2 July 2022

Accepted: 22 October 2022

Published: 24 October 2022

Publisher's Note: MDPI stays neutral with regard to jurisdictional claims in published maps and institutional affiliations.



Copyright: © 2022 by the authors. Licensee MDPI, Basel, Switzerland. This article is an open access article distributed under the terms and conditions of the Creative Commons Attribution (CC BY) license (<https://creativecommons.org/licenses/by/4.0/>).

1. Introduction

As we enter yet another era of global conflicts, wounds are an unfortunate and an inevitable consequence from the ruthless battlefield. In such an event, immediate medical attention becomes absolutely necessary to ease inextricable physiological pain and emotional pain [1]. The high morbidity and mortality related to combat wounds are mainly due to uncontrolled hemorrhage and bacterial infections. Hemostatic and antibacterial characteristics, therefore, become a fundamental prerequisite for wound dressing materials [2,3].

From outdated medical cotton gauze to highly sophisticated moisture-balanced dressings, various types of dressings, including hydrogels [4,5], tissue adhesives [6–8], foams [9,10], alginates [11,12], and silicone-based materials [13,14], have been investigated to determine the optimum conditions in the wound healing processes [15,16]. Certain characteristics are needed for improved healing processes, which includes moisture-control, air permeability, exudate removal, antimicrobial, mechanical stability/elasticity, and biocompatibility/biodegradability [16]. In this study, Tencel, also known as lyocell, is used. It is known as an environment-friendly regenerated cellulose fiber used in textile research to enhance comfortable and breathable sensations [17,18]. It is also commonly adopted by the textile industry as a preferred material for fabricating garments such as sportswear, underwear, outerwear [18], and IoT-enabled smart clothing [19,20]. Over the past decade, extensive studies on moisture-wicking [21], softness [22], and enhanced mechanical behaviors [23] in Tencel have also opened up potential applications in wound dressings [24,25]. Tencel can not only fulfill most of the characteristics mentioned in the prior description, it is also cost effective, which makes production possible.

Tencel, however, has a drawback in its antimicrobial characteristics, which is usually expected in cellulose-based materials. In order to address this issue, researchers with pharmaceutical knowledge would likely adopt the idea of using antibiotics, such as ciprofloxacin [26], gentamicin [27], and mupirocin [28], as an antimicrobial additive. The

incorporation of antibiotics can effectively deliver high concentrations of microbe-specific substances to local infectious sites, as suggested by Ramasubbu et al. [29]. However, there are cases where high amounts of antibiotics can cause long-lasting neurological damages [30]. Material scientists, on the other hand, are keener toward the use of different sorts of nanoparticles, such as silver [31–34], gold [35–37], metal oxides [38–40], and other metal-based compounds [41,42], to prevent bacterial infections and to overcome antimicrobial resistance (AMR) caused by the overuse and misuse of antibiotics.

To further reinforce the biofunction of Tencel, a bioactive agent has been implemented, as inspired by many studies on the strategic design of recent wound dressings [43]. It is evident that bioactive agents can induce or stimulate re-epithelialization on wound sites [44,45]. Although theoretical mechanisms are yet to be proven, many explanations have shown a certain depth of correlation with cell regulation on migration [46] and proliferation [47]. Other functions, such as anti-inflammatory from plant-based substances, have also been reported to be a potent tactic on epithelialization [48–52]. Researchers also attempted to alleviate the inflammatory response and support the healing process with different types of vitamins [53–56].

An ultimate challenge in the process of adding antimicrobial or bioactive agents would be the presence of more solvents or emulsifiers that could jeopardize the construction of suitable biocompatible scaffolds, and sacrifice the intended functionalities in various fabrication techniques. Eulálio et al. showed that the use of different organic acids has great impact on the physicochemical properties of chitosan [57]. Electrospun polymer-titanium dioxide nanocomposites, prepared by Ghosal et al., revealed the critical point for dispersion of nanoparticles, polymer spinnability, and the suitable application in biomedicine [58]. In addition, Fahimirad et al. demonstrated the use ethanol, methanol, and acetic acid for preparing multi-component, multi-layered structure membranes with antibacterial, antioxidant activity, and cytotoxicity effects on human epidermal cells [59].

Herein, the fabrication, characterization, and biological properties of peptide-coated nano-CuO/Tencel membranes for potential application in treating wounds are reported. The effects of atmospheric argon plasma treatment time on bioactive peptide coating on Tencel fibers are also evaluated. The prepared samples were characterized by scanning electron microscopy (SEM), Fourier-transform infrared (FT-IR) spectroscopy, contact angle measurement, and a variety of in vitro cell assays and antimicrobial assessments against skin-infection-related bacteria: Gram-negative *E. coli* and Gram-positive *S. aureus*.

2. Materials and Methods

2.1. Materials

Tencel[®] fibers (purchased from Asiatic Fiber Corporation, Taipei, Taiwan) and highly concentrated 800-ppm proprietary bioactive peptide (acquired from Taiwan Goodwill Murray Peptide Technologies, Inc., Taipei, Taiwan) were used as received without further purification. Copper oxide nanoparticles were prepared by a green and rapid synthesis method, described in our previous work, such that zero hazardous substances were used or generated from the synthesis process [60].

2.2. Membranes Fabrication

A schematic illustration of the peptide coated nano-CuO/Tencel membrane fabrication is shown in Figure 1. Tencel fibers underwent a series of fiber processing from blending, carding, and needle-punching to produce a nonwoven Tencel sheet (basis weight: 100 g/m²) [61]. The nonwoven sheet was then immersed in deionized water with 4 wt.% copper oxide nanoparticle suspension, for optimal particle adhesion and an antimicrobial effect, onto Tencel fiber surface, followed by drying at room temperature for 4 h. A modified atmospheric pressure plasma jet system with a voltage of 45 kV, argon flow rate of 5 SLM, and a peptide injection flow rate of 0.05 L/min was used to coat bioactive peptide onto the nano-CuO/Tencel surface, where the tip of the plasma jet was placed 2 cm above the

Tencel sheet. The peptide treatment time was set at 0, 30, 60, 90, and 120 s. The samples were kept in a desiccator up to three days before performing characterizations.

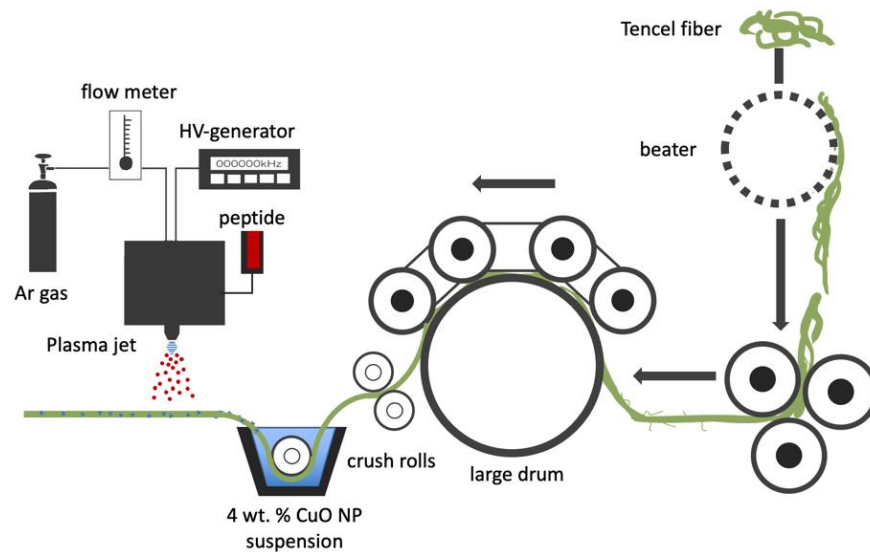


Figure 1. Schematic of the fabrication sequence of peptide-coated nano-CuO/Tencel.

2.3. Scanning Electron Microscopy (SEM)

The surface morphology of the fabricated nano-CuO/Tencel with bioactive peptide coating was characterized. The samples were sputter-coated with gold, and viewed under a Hitachi (S-3400N, Tokyo, Japan) scanning electron microscope (SEM) at an accelerating voltage between 5 and 20 kV, and mounted with energy dispersive X-ray analysis (EDX) in the Precision Instruments Support Center, Feng Chia University. Micrographs were collected at magnification of 1k \times and 5k \times using secondary electrons and backscattered electrons.

2.4. Fourier-Transform Infrared Spectroscopy (FT-IR)

Transmission Fourier-transform infrared (FT-IR) spectroscopic measurements were performed on a Fourier-transform infrared spectrophotometer (Thermo Nicolet iS5 FTIR, Waltham, MA, USA) in National Cheng Kung University. All the FT-IR measurements were repeated three times for each sample, and are well reproducible.

2.5. Contact Angle Measurements

The contact angle was measured using a static method and direct measurement of the tangent angle, θ , at the three-phase contact point on a sessile drop profile, using high-resolution photographs of pure water drops and a graphic processing software supplied by the manufacturer of the contact angle meter (CAM-100, Creating Nano Technologies Inc., Tainan, Taiwan). When θ is higher than 90 $^\circ$, the surface is hydrophobic, whereas it is hydrophilic when the angle is less than 90 $^\circ$.

2.6. Cytotoxicity Evaluation

L929 standard fibroblasts (ATCC cell line) were cultured in Dulbecco's modified Eagle's medium (DMEM) and supplemented with 10% fetal bovine serum (FBS) and 1% penicillin-streptomycin. Cells were maintained at 37 $^\circ$ C in a humidified incubator with 5% CO₂ for 24 h, until about 80% confluence was obtained. Cell counts were standardized.

The prepared membranes ($n = 3$) were placed into 24-well tissue culture polystyrene plates without further treatment. After UV irradiation sterilization, cells were seeded at a density of 1 $\times 10^5$ cells/cm² in each well plate. Cellular viability was assessed using a 3-(4,5-dimethylthiazol-2-yl)-2,5-diphenyltetrazolium bromide (MTT) assay taken after 24 h. The culture medium was discarded, followed by washing with PBS twice and incubation

with MTT solution at 37 °C for 4 h. The formazan crystals were dissolved in dimethyl sulfoxide (DMSO), and optical activity was measured at 570 nm with an ELISA reader.

2.7. Antimicrobial Assay

The inhibitory effects of copper-tailored membranes on the bacterial growth were estimated by means of turbidity measurements. The reference bacterial broth (3×10^8 bacteria/mL) was used as a standard sample. Selected membranes (1 cm \times 1 cm) were cultured in *E. coli* (six-fold serial dilution) and *S. aureus* (four-fold serial dilution) bacterial broth at room temperature for 24 h. The optical density (OD) of all solutions was measured with an UV/VIS spectrophotometer (JASCO V-550) at 620 nm.

3. Results and Discussion

3.1. Surface Morphology of Nano-CuO/Tencel Membranes

The surface morphology of the prepared Tencel fibers were studied by SEM. This technique enabled us to examine the effect of plasma treatment on a single fiber in the fabrication sequence. Plasma treatment resulted in extensive changes of the Tencel surface morphology. Figure 2 shows SEM images of pristine Tencel, CuO-coated Tencel, and peptide-included CuO/Tencel fibers with different plasma treatment times. Pristine Tencel fibers appear to have a smooth fiber surface with an average diameter around 18 μm (Figure 2a). As shown in Figure 2b–g it is revealed that fiber diameters ranging from 15–22 μm are observed in Tencel fibers impregnated with CuO particulate, whereas no significant change in fiber diameter is observed for peptide-coated fibers (Figure 2c–g). Apparent CuO nanocrystals can be seen in Figure 2b (indicated with an arrow), with the inset showing elemental values in percentage. No noticeable change is observed when increasing the argon plasma treatment time from 0 to 60 s (Figure 2c–e); however, a slightly roughened surface morphology becomes visible with 90 s exposure time (Figure 2f). When plasma exposure time is further extended to 120 s, severe stripping on the fiber surface is detected in Figure 2g, where evidence of partial deterioration is clearly seen in the close-up view (Figure 2h). The observed surface changes and stripped fibers are the consequence of sample ablation during plasma treatment [62–64]. The fibers create a greater surface area in comparison to the smooth surface of pristine Tencel fibers. As reported by Lewis et al., larger surface area is responsible for superior hemostatic properties [65].

3.2. FT-IR Analysis of Nano-CuO/Tencel Membranes

The FT-IR spectra for nano-CuO/Tencel membranes with different plasma exposure times were recorded in the range of 4000–400 cm^{-1} . As shown in Figure 3, the FT-IR spectra of Tencel fabric show distinctive peaks, including O-H stretching at 3399 cm^{-1} , C-H stretching at 2985 cm^{-1} , O-H bending at 1633 cm^{-1} , CH₂ bending at 1427 cm^{-1} , and the C-H bending at 1387 cm^{-1} [66]. These peaks are the characteristic peaks of cellulose. The observed peaks at 453, 494, and 609 cm^{-1} (in dashed circle) correspond to the characteristic stretching vibrations in CuO [67]. It is observed that such IR feature is not particularly distinctive when peptide is added. Generally speaking, the absorbance in the amide region has a strong correlation to the amino side chain in collagen or peptide [68,69]. It is assumed that the absorbance of 1635 cm^{-1} mainly arises from amide contribution [70]. This spectral feature is particularly obvious in the Tencel+CuO+Peptide_30s-90s samples. In samples treated with plasma, the band at 1749 cm^{-1} corresponds to -C=O in -COOH. The presence of carboxyl groups in these spectra is the result of plasma treatment [71]. According to the results, the amino groups of the peptide forms the Schiff-base structure onto the Tencel fiber surface, which aligns with the IR absorbance at 1635 cm^{-1} (Figure 4) [72]. As the fibers are progressively etched (Tencel+CuO+Peptide_120s), the amide I and -C=O bands become reduced or diminished. In addition, the strong absorption bands between 3500–4000 cm^{-1} and 1624 cm^{-1} (overlapped with O-H bending) are allocated to the presence of water molecules that are absorbed on the high surface-to-volume ratio nanostructures [73,74].

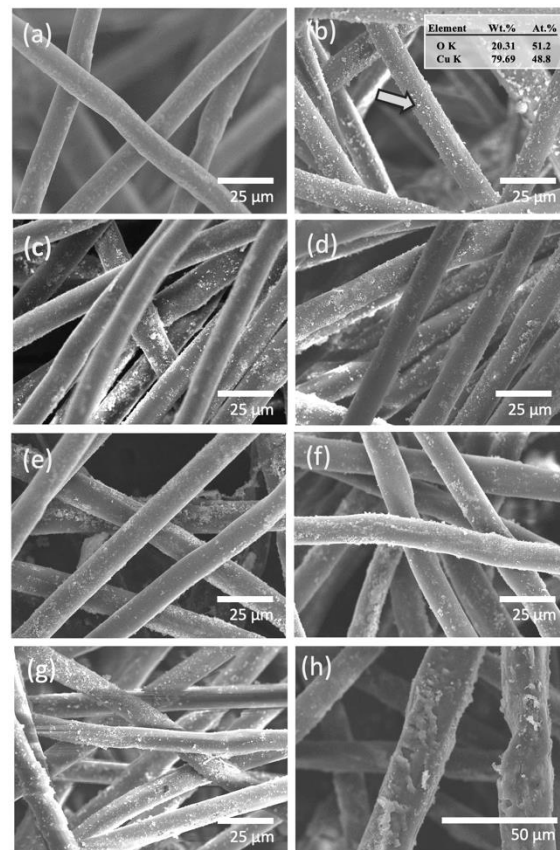


Figure 2. Scanning electron microscopy images of (a) Tencel; (b) Tecenl+CuO; and Tecenl+CuO+peptide (c) 0, (d) 30, (e) 60, (f) 90, and (g,h) 120 s of argon plasma treatment time at low and high magnification.

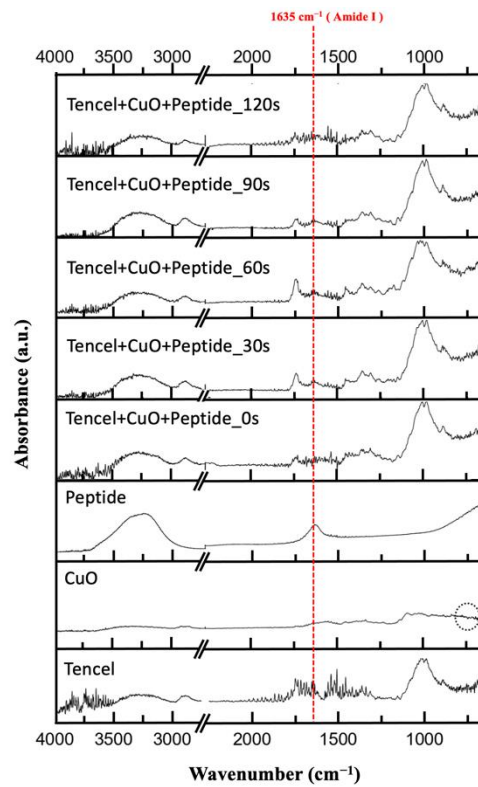


Figure 3. FT-IR spectra of nano-CuO/Tencel membranes with different plasma treatment times.

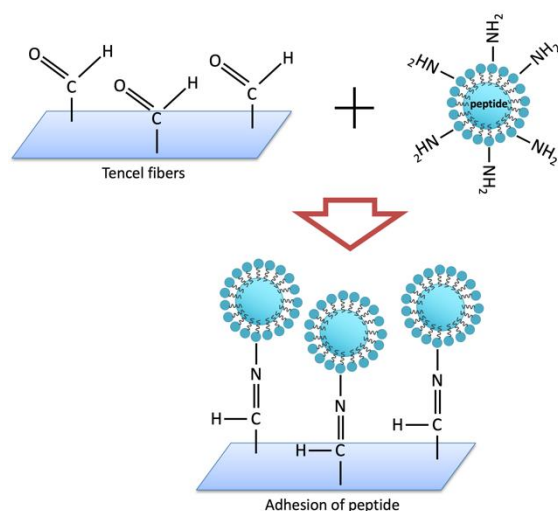


Figure 4. Schematic illustration of formation mechanism of peptide onto Tencel membranes.

3.3. Cytotoxicity and Contact Angle Measurements of Nano-CuO/Tencel Membranes

An effective wound dressing material must be non-cytotoxic to the relevant cell to maintain viability at the wound site. To reveal the cyto-compatibility of the tested membranes, the cell viability of the L929 fibroblastic cells was investigated. The L929 cell line is one of the most frequently used lines in material/cell interaction research, and has been previously used for cytotoxicity testing for many polymeric scaffolds [75–77]. The cytotoxicity and wettability of the prepared membranes are summarized in Figure 5. Tencel is extremely hydrophilic, and the high wetting behavior is primarily attributed to the -OH group from the cellulose-based structure (blue circles in Figure 5) [73]. Moreover, Tencel fibers pose no adverse effect on fibroblastic cells, such that the cell viability is very similar to that of the control sample. In Tencel+CuO, CuO nanoparticles appear to have a high cytotoxicity, whereas peptide-added samples appear to have little or no cytotoxic effect. Others also demonstrated a similar outcome that copper(II) complex or copper oxide nanoparticles have toxicity against L929 mouse fibroblast, A549 human lung cancer cells, or to DNA from reactive oxygen species (ROS), which enables us to comprehend apoptosis induction or an anti-proliferation effect of CuO in Tencel membranes [78–80]. Fibroblasts (NIH/3T3) induced with bioactive peptide show a faster gap closure rate (Figure A1A), whereas the quantitative result reveals a slower cell migration without peptide treatment (square curve) compared to peptide-treated cells (circle curve). A significant split in wound area difference is seen at 6 h, and reaches its maximum at around 13 h where the wound area is almost closed (Figure A1B). The assessment, however, was not performed on the peptide-CuO/Tencel samples because of technical limitations. The effects of the peptide-grafted Tencel samples on cell viability can be associated and explained by the degree of peptide adhesion from plasma treatment according to the IR results from Tencel+CuO+Peptide_30s-90s samples.

3.4. Antimicrobial Activity

One of the pivotal factors to accelerate wound healing is the ability to impede microbial infections [81,82]. Therefore, copper oxide nanoparticles were introduced as an inorganic antimicrobial agent. The antimicrobial behaviors of the devised nano-CuO/Tencel membranes against *E. coli* and *S. aureus* were evaluated as optical density (OD) measurements, as presented in Figure 6. The antimicrobial nature of copper oxides is also clearly observed against both Gram-positive and -negative bacterial strains [83]. For both bacterial solutions exposed to nano-CuO-coated Tencel surfaces, the absorbance readings are reduced, indicating that these surfaces can inhibit bacteria growth in a liquid medium. The inhibitory action is more obvious for Gram-negative bacteria, as the overall absorbance in Gram-positive bacteria is much higher. The results suggest an electrostatic interac-

tion between positively charged copper ions that disrupts the membrane integrity of the Gram-negative bacteria [84]. As expected from the cytotoxicity test, the presence of peptide also shows similar patterns for plasma-treated samples in the antimicrobial results. As peptide is being applied onto the nano-CuO/Tencel fibers, argon ions are initiating reactive species for reaction and etching newly established bonds simultaneously [85]. Thus, the absorbance readings for both bacteria begin to decline at 90 s plasma treatment time, mainly because of the competing result of grafting and removing of peptide that leads to the protrusion of copper oxide for antimicrobial activity. The stripped fibers at 120 s of plasma treatment time ultimately deteriorated, and demonstrated unstable and inconsistent antimicrobial capability.

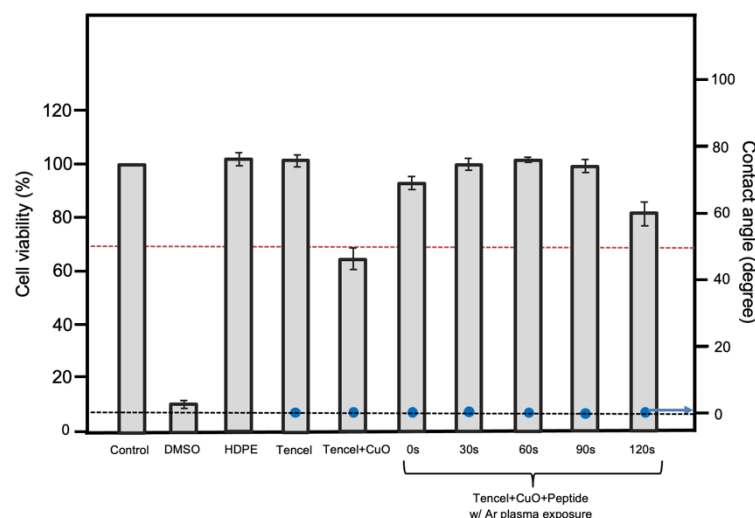


Figure 5. Cytotoxicity (red dashed line indicates 70% viability) and contact angle measurement (black dashed line indicates zero degree) of the Tencel membranes.

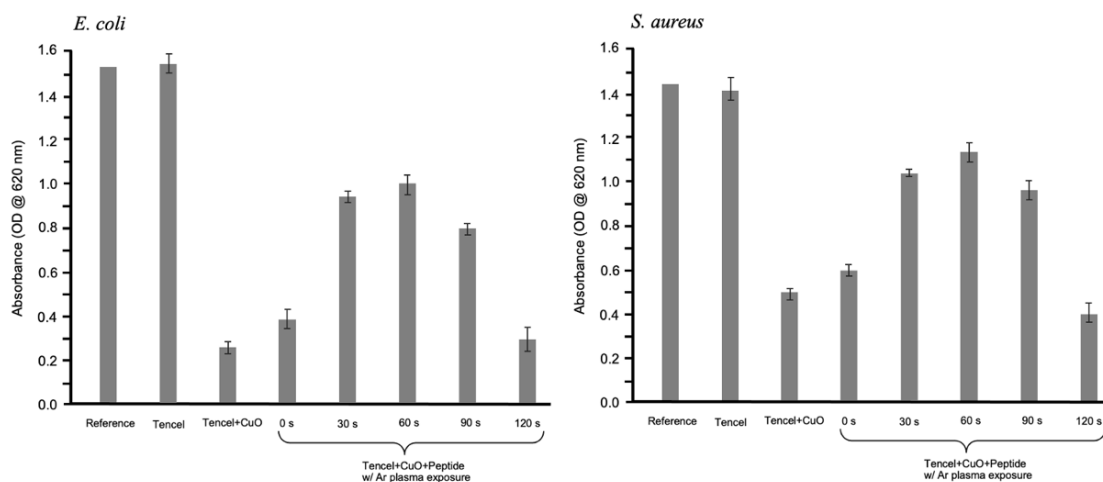


Figure 6. Absorbance, as measured at 620 nm, of *E. coli* (left) and *S. aureus* (right) bacterial broth exposed to various membranes.

4. Conclusions

An innovative method to graft bioactive peptide onto nano-CuO/Tencel membranes has been proposed. The results have revealed that membranes remain high fiber surface integrity between 30 and 60 s of plasma treatment time. Though slight roughness is observed at 90 s that etches off peptide partially to promote antimicrobial activity against *E. coli* and *S. aureus*, cell viability with fibroblastic cells is still maintained. Ongoing experiments, including peptide adhesion on the fiber surface, and its cellular response mechanism, shall be carefully investigated for future publication.

Author Contributions: Conceptualization, validation, supervision, writing, J.H.C.Y., S.-C.S. and T.-L.H.; methodology, formal analysis, G.-Y.C. All authors have read and agreed to the published version of the manuscript.

Funding: This research was funded by Jen-Ai Hospital, grant number 512509C1011T.

Institutional Review Board Statement: Not applicable.

Informed Consent Statement: Not applicable.

Data Availability Statement: Not applicable.

Acknowledgments: The authors thank J.H. Lin of the Laboratory of Fiber Application and Manufacturing, Feng Chia University, for their expert fabrication techniques. The authors also thank Taiwan Goodwill Murray Peptide Technologies, Inc. for supplying the bioactive peptide.

Conflicts of Interest: The authors declare no conflict of interest.

Appendix A

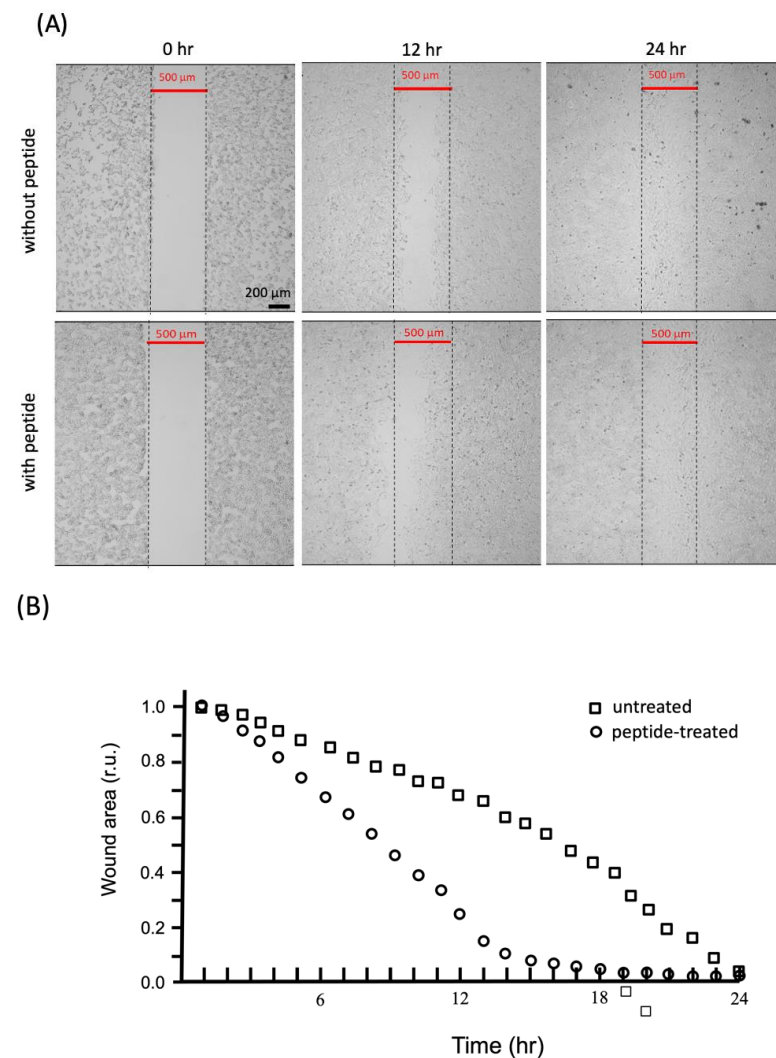


Figure A1. Analysis of NIH/3T3 fibroblastic cell migration by in vitro wound-healing assay. (A) Time-lapse microscopy images of wound closure of untreated (without peptide) and treated with peptide NIH/3T3 fibroblasts at 0, 12, and 24 h after culture insert removal. (B) Quantification of the wounded area during 24 h by untreated (square curve) and treated with peptide (circle curve) NIH/3T3 fibroblasts, presented in relative units (r.u.).

References

1. Gulland, A. Emergency Medicine: Lessons from the battlefield. *BMJ* **2008**, *336*, 1098–1100. [[CrossRef](#)] [[PubMed](#)]
2. Tamer, T.M.; Sabet, M.M.; Omer, A.M.; Abbas, E.; Eid, A.I.; Hohy-Eldin, M.S.; Hassan, M. Hemostatic and antibacterial PVA/Kaolin composite sponges loaded with penicillin–streptomycin for wound dressing applications. *Sci. Rep.* **2021**, *11*, 3428. [[CrossRef](#)] [[PubMed](#)]
3. Wu, Z.; Zhou, W.; Deng, W.; Xu, C.; Cai, Y.; Wang, X. Antibacterial and Hemostatic Thiol-Modified Chitosan-Immobilized AgNPs Composite Sponges. *ACS Appl. Mater. Interfaces* **2020**, *12*, 20307–20320. [[CrossRef](#)] [[PubMed](#)]
4. Liang, Y.; He, J.; Guo, B. Functional Hydrogels as Wound Dressing to Enhance Wound Healing. *ACS Nano* **2021**, *15*, 12687–12722. [[CrossRef](#)] [[PubMed](#)]
5. Tavakoli, S.; Klar, A. Advanced Hydrogels as Wound Dressings. *Biomolecules* **2020**, *10*, 1169. [[CrossRef](#)] [[PubMed](#)]
6. Li, M.; Zhang, Z.; Liang, Y.; He, J.; Guo, B. Multifunctional Tissue-Adhesive Cryogel Wound Dressing for Rapid Nonpressing Surface Hemorrhage and Wound Repair. *ACS Appl. Mater. Interfaces* **2020**, *12*, 35856–35872. [[CrossRef](#)] [[PubMed](#)]
7. Quinn, J.; Mertz, M. The effect of a new tissue-adhesive wound dressing on the healing of traumatic abrasions. *Dermatology* **2000**, *201*, 343–346. [[CrossRef](#)]
8. Nishiguchi, A.; Taguchi, T. Designing an anti-inflammatory and tissue-adhesive colloidal dressing for wound treatment. *Colloids Surf. B Biointerfaces* **2020**, *188*, 110737. [[CrossRef](#)]
9. Kirwan, H.; Pignataro, R. The Skin and Wound Healing. In *Pathology and Intervention in Musculoskeletal Rehabilitation*, 2nd ed.; Elsevier: London, UK, 2016; pp. 25–62.
10. Weller, C. Interactive dressings and their role in moist wound management. In *Advanced Textiles for Wound Care*; Woodhead Publishing: Sawston, UK, 2009; pp. 97–113.
11. Aderibigbe, B.; Byuana, B. Alginate in Wound Dressings. *Pharmaceutics* **2018**, *10*, 42. [[CrossRef](#)]
12. Weigelt, M.A.; Sanchez, D.P.; Lev-Tov, H. Dressings and Wound Care Supplies for Hidradenitis Suppurativa. In *A Comprehensive Guide to Hidradenitis Suppurativa*; Elsevier: London, UK, 2022; pp. 201–207.
13. Derbyshire, A. Using a silicone-based dressing as a primary wound contact layer. *Br. J. Nurs.* **2014**, *23*, S14–S20. [[CrossRef](#)]
14. Morris, C.; Emsley, P.; Marland, E.; Meuleneire, F.; White, R. Use of wound dressings with soft silicone adhesive technology. *Paediatr. Nurs.* **2009**, *21*, 38–43. [[PubMed](#)]
15. Boateng, J.S.; Matthews, K.H.; Stevens, H.N.E.; Eccleston, G.M.J. Wound healing dressings and drug delivery systems: A review. *Pharm. Sci.* **2008**, *97*, 2892. [[CrossRef](#)]
16. Jain, S.; Domb, A.J.; Kumar, N. *Focal Controlled Drug Delivery*; Domb, A.J., Khan, W., Eds.; Springer: Dordrecht, The Netherlands, 2014; p. 585.
17. Kim, H. Moisture Vapor Permeability and Thermal Wear Comfort of Ecofriendly Fiber-Embedded Woven Fabrics for High-Performance Clothing. *Materials* **2021**, *14*, 6205. [[CrossRef](#)] [[PubMed](#)]
18. Badr, A.A.; El-Nahrawy, A.; Hassanin, A.; Morsy, M. Comfort and Protection Properties of Tencel/Cotton Blends. In *Beltwide Cotton Conference Proceedings*; National Cotton Council Omnipress: Madison, WI, USA, 2014.
19. Gomez, M.; Alvarez, H.; Berdasco, A.; Andres, F. Paving the Way to Eco-Friendly IoT Antennas: Tencel-Based Ultra-Thin Compact Monopole and Its Applications to ZigBee. *Sensors* **2020**, *20*, 3658. [[CrossRef](#)]
20. Felgueiras, C.; Azoia, N.G.; Gonçalves, C.; Gama, M.; Dourado, F. Trends on the Cellulose-Based Textiles: Raw Materials and Technologies. *Front. Bioeng. Biotechnol.* **2021**, *9*, 608826. [[CrossRef](#)] [[PubMed](#)]
21. Karthikeyan, J.G.; Nalakilli, G.; Shanmugasundaram, O.L.; Prakash, C. Moisture Management Properties of Bamboo Viscose/Tencel Single Jersey Knitted Fabrics. *J. Nat. Fibers* **2016**, *14*, 143–152. [[CrossRef](#)]
22. Zhang, Q.; Zhou, R. The Study of Moisture Absorption and Release Properties of Tencel Fiber. *Adv. Mater. Res.* **2012**, *627*, 138–142. [[CrossRef](#)]
23. Firgo, H.; Schuster, K.C.; Suchomel, F.; Männer, J.; Burrow, T.; Abu-Rous, M. The functional properties of Tencel—A current update. *Lenzing. Ber.* **2006**, *85*, 22–30.
24. Lou, C.W.; Lin, J.H.; Lai, M.F.; Huang, C.H.; Shiu, B.C. Lay-Up Compound Matrices for Application of Medical Protective Clothing: Manufacturing Techniques and Property Evaluations. *Polymers* **2022**, *14*, 1179. [[CrossRef](#)]
25. Li, T.; Lou, C.; Chen, A.; Lee, M.; Ho, T.; Chen, Y.; Lin, J. Highly Absorbent Antibacterial Hemostatic Dressing for Healing Severe Hemorrhagic Wounds. *Materials* **2016**, *9*, 793. [[CrossRef](#)]
26. Li, H.; Williams, G.R.; Wu, J.; Lv, Y.; Sun, X.; Wu, H.; Zhu, L.M. Thermosensitive nanofibers loaded with ciprofloxacin as antibacterial wound dressing materials. *Int. J. Pharm.* **2017**, *517*, 135–147. [[CrossRef](#)] [[PubMed](#)]
27. Bakhsheshi-Rad, H.R.; Hadisi, Z.; Ismail, A.F.; Aziz, M.; Akbari, M.; Berto, F.; Chen, X.B. In vitro and in vivo evaluation of chitosan-alginate/gentamicin wound dressing nanofibrous with high antibacterial performance. *Polym. Test* **2020**, *82*, 106298. [[CrossRef](#)]
28. Li, X.; Wang, C.; Yang, S.; Liu, P.; Zhang, B. Electrospun PCL/mupirocin and chitosan/lidocaine hydrochloride multifunctional double layer nanofibrous scaffolds for wound dressing applications. *Int. J. Nanomed.* **2018**, *13*, 5287. [[CrossRef](#)] [[PubMed](#)]
29. Ramasubbu, D.A.; Smith, V.; Hayden, F.; Cronin, P. Systemic antibiotics for treating malignant wounds. *Cochrane Database Syst. Rev.* **2017**, *8*, CD011609. [[CrossRef](#)]
30. Marchant, J. When antibiotics turn toxic. *Nature* **2018**, *555*, 431–433. [[CrossRef](#)] [[PubMed](#)]

31. Choi, J.S.; Jung, H.C.; Baek, Y.J.; Kim, B.Y.; Lee, M.W.; Kim, H.D.; Kim, S.W. Antibacterial Activity of Green-Synthesized Silver Nanoparticles Using Areca catechu Extract against Antibiotic-Resistant Bacteria. *Nanomaterials* **2021**, *11*, 205. [[CrossRef](#)]
32. Soliman, W.E.; Khan, S.; Rizvi, S.M.D.; Moin, A.; Elsewedy, H.S.; Abulila, A.S.; Shehata, T.M. Therapeutic Applications of Biostable Silver Nanoparticles Synthesized Using Peel Extract of *Benincasa hispida*: Antibacterial and Anticancer Activities. *Nanomaterials* **2020**, *10*, 1954. [[CrossRef](#)]
33. Tormena, R.P.; Rosa, E.V.; Mota, B.; Chaker, J.; Fagg, C.W.; Freire, D.O.; Martins, P.M.; Rodrigues da Silva, I.C.; Sousa, M.H. Evaluation of the antimicrobial activity of silver nanoparticles obtained by microwave-assisted green synthesis using *Handroanthus impetiginosus* (Mart. ex DC.) Mattos underbark extract. *RSC Adv.* **2020**, *10*, 20676–20681. [[CrossRef](#)] [[PubMed](#)]
34. Urnukhsaikhan, E.; Bold, B.E.; Gunbileg, A.; Sukhbaatar, N.; Mishig-Ochir, T. Antibacterial activity and characteristics of silver nanoparticles biosynthesized from *Carduus crispus*. *Sci. Rep.* **2021**, *11*, 21047. [[CrossRef](#)]
35. Shamaila, S.; Zafar, N.; Riaz, S.; Sharif, R.; Nazir, J.; Naseem, S. Gold Nanoparticles: An Efficient Antimicrobial Agent against Enteric Bacterial Human Pathogen. *Nanomaterials* **2016**, *6*, 71. [[CrossRef](#)]
36. Sathiyaraj, S.; Suriyakala, G.; Gandhi, A.D.; Babujanarthanam, R.; Almaary, K.S.; Chen, T.W.; Kaviyarasu, K. Biosynthesis, characterization, and antibacterial activity of gold nanoparticles. *J. Infect. Public Health* **2021**, *14*, 1842–1847. [[CrossRef](#)] [[PubMed](#)]
37. Tao, C. Antimicrobial activity and toxicity of gold nanoparticles: Research progress, challenges and prospects. *Lett. Appl. Microbiol.* **2018**, *67*, 537–543. [[CrossRef](#)] [[PubMed](#)]
38. Siddiqi, K.S.; Rahman, A.; Tajuddin; Husen, A. Properties of Zinc Oxide Nanoparticles and Their Activity against Microbes. *Nanoscale Res. Lett.* **2018**, *13*, 141. [[CrossRef](#)] [[PubMed](#)]
39. de Dicastillo, C.L.; Correa, M.G.; Martínez, F.B.; Streitt, C.; Galotto, M.J. Antimicrobial Effect of Titanium Dioxide Nanoparticles. In *Antimicrobial Resistance*; InTechOpen: London, UK, 2020.
40. Azizi-Lalabadi, M.; Ehsani, A.; Divband, B.; Alizadeh-Sani, M. Antimicrobial activity of Titanium dioxide and Zinc oxide nanoparticles supported in 4A zeolite and evaluation the morphological characteristic. *Sci. Rep.* **2019**, *9*, 17439. [[CrossRef](#)] [[PubMed](#)]
41. Lee, M.-J.; Seo, Y.-B.; Seo, J.-Y.; Ryu, J.-H.; Ahn, H.-J.; Kim, K.-M.; Kwon, J.-S.; Choi, S.-H. Development of a Bioactive Flowable Resin Composite Containing a Zinc-Doped Phosphate-Based Glass. *Nanomaterials* **2020**, *10*, 2311. [[CrossRef](#)]
42. Pop, O.L.; Mesaros, A.; Vodnar, D.C.; Suharoschi, R.; Tăbăran, F.; Mageruşan, L.; Tódor, I.S.; Diaconeasa, Z.; Balint, A.; Ciontea, L.; et al. Cerium Oxide Nanoparticles and Their Efficient Antibacterial Application In Vitro against Gram-Positive and Gram-Negative Pathogens. *Nanomaterials* **2020**, *10*, 1614. [[CrossRef](#)]
43. Simões, D.; Miguel, S.P.; Ribeiro, M.P.; Coutinho, P.; Mendonça, A.G.; Correia, I.J. Recent advances on antimicrobial wound dressing: A review. *Eur. J. Pharm. Biopharm.* **2018**, *127*, 130–141. [[CrossRef](#)]
44. Liang, J.; Cui, L.; Li, J.; Guan, S.; Zhang, K.; Li, J. Aloe vera: A Medicinal Plant Used in Skin Wound Healing. *Tissue Eng. Part B Rev.* **2021**, *27*, 455–474. [[CrossRef](#)]
45. Pastar, I.; Stojadinovic, O.; Yin, N.C.; Ramirez, H.; Nusbaum, A.G.; Sawaya, A.; Patel, S.B.; Khalid, L.; Isseroff, R.R.; Tomic-Canic, M. Epithelialization in Wound Healing: A Comprehensive Review. *Adv. Wound Care* **2014**, *3*, 445–464. [[CrossRef](#)]
46. Werner, S.; Grose, R. Regulation of wound healing by growth factors and cytokines. *Physiol. Rev.* **2003**, *83*, 835. [[CrossRef](#)]
47. Gniadecki, R. Regulation of keratinocyte proliferation. *Gen. Pharmacol.* **1998**, *30*, 619. [[CrossRef](#)]
48. Gupta, A.; Keddie, D.J.; Kannappan, V.; Gibson, H.; Khalil, I.R.; Kowalczyk, M.; Martin, C.; Shuai, X.; Radecka, I. Production and characterisation of bacterial cellulose hydrogels loaded with curcumin encapsulated in cyclodextrins as wound dressings. *Eur. Polym. J.* **2019**, *118*, 437–450. [[CrossRef](#)]
49. Mutlu, G.; Calamak, S.; Ulubayram, K.; Guven, E. Curcumin-loaded electrospun PHBV nanofibers as potential wound-dressing material. *J. Drug Deliv. Sci. Technol.* **2018**, *43*, 185–193. [[CrossRef](#)]
50. Jiji, S.; Udhayakumar, S.; Rose, C.; Muralidharan, C.; Kadirvelu, K. Thymol enriched bacterial cellulose hydrogel as effective material for third degree burn wound repair. *Int. J. Biol. Macromol.* **2019**, *122*, 452–460. [[CrossRef](#)]
51. Chen, Y.; Qiu, Y.; Chen, W.; Wei, Q. Electrospun thymol-loaded porous cellulose acetate fibers with potential biomedical applications. *Mater. Sci. Eng. C* **2020**, *109*, 110536. [[CrossRef](#)]
52. Lee, K.; Lee, S. Electrospun Nanofibrous Membranes with Essential Oils for Wound Dressing Applications. *Fibers Polym.* **2020**, *21*, 999–1012. [[CrossRef](#)]
53. Vivcharenko, V.; Wojcik, M.; Palka, K.; Przekora, A. Highly Porous and Superabsorbent Biomaterial Made of Marine-Derived Polysaccharides and Ascorbic Acid as an Optimal Dressing for Exuding Wound Management. *Materials* **2021**, *14*, 1211. [[CrossRef](#)]
54. Farzanfar, S.; Kouzekonan, G.S.; Mirjani, R.; Shekarchi, B. Vitamin B12-loaded polycaprolacton/gelatin nanofibrous scaffold as potential wound care material. *Biomed. Eng. Lett.* **2020**, *10*, 547–554. [[CrossRef](#)]
55. Ehterami, A.; Salehi, M.; Farzamfar, S.; Samadian, H.; Vaez, A.; Sahrpeyma, H.; Ghorbani, S. A promising wound dressing based on alginate hydrogels containing vitamin D3 cross-linked by calcium carbonate/d-glucono- δ -lactone. *Biomed. Eng. Lett.* **2020**, *10*, 309–319. [[CrossRef](#)]
56. Li, H.; Wang, M.; Williams, G.R.; Wu, J.; Sun, X.; Lv, Y.; Zhu, L.-M. Electrospun gelatin nanofibers loaded with vitamins A and E as antibacterial wound dressing materials. *RSC Adv.* **2016**, *6*, 50267–50277. [[CrossRef](#)]

57. Eulálio, H.Y.C.; Vieira, M.; Fideles, T.B.; Tomás, H.; Silva, S.M.L.; Peniche, C.A.; Fook, M.V.L. Physicochemical Properties and Cell Viability of Shrimp Chitosan Films as Affected by Film Casting Solvents. I-Potential Use as Wound Dressing. *Materials* **2020**, *13*, 5005. [[CrossRef](#)] [[PubMed](#)]
58. Ghosal, K.; Agatemor, C.; Špitálský, Z.; Thomas, S.; Kny, E. Electrospinning tissue engineering and wound dressing scaffolds from polymer-titanium dioxide nanocomposites. *Chem. Eng. J.* **2019**, *358*, 1262–1278. [[CrossRef](#)]
59. Fahimirad, S.; Abtahi, H.; Satei, P.; Ghaznavi-Rad, E.; Moslehi, M.; Ganji, A. Wound healing performance of PCL/chitosan based electrospun nanofiber electrospayed with curcumin loaded chitosan nanoparticles. *Carbohydr. Polym.* **2021**, *259*, 117640. [[CrossRef](#)] [[PubMed](#)]
60. Yang, J.H.C.; Wu, S.-L.; Tsai, C.-S. Green and Rapid Fabrication of Copper Oxide in Enhanced Electrode Liquid Phase Plasma System. *Plasma Process. Polym.* **2022**, e2200078. [[CrossRef](#)]
61. Lou, C.W.; Lu, C.T.; Chen, Y.S.; Lin, M.C.; Li, T.T.; Lin, J.H. The Primary Study on PLA/Tencel Nonwoven Fabric. *Appl. Mech. Mater.* **2012**, *184–185*, 1333–1336. [[CrossRef](#)]
62. Gomathi, N.; Chanda, A.K.; Neogi, S. Atmospheric Plasma Treatment of Polymers for Biomedical Applications. In *Atmospheric Pressure Plasma Treatment of Polymers: Relevance to Adhesion*; Scrivener Publishing: Salem, MA, USA, 2013.
63. Švorčík, V.; Hnatowicz, V. Properties of polymers modified by plasma discharge and ion beam. In *Polymer Degradation and Stability*; Nova Science Publishers: New York, NY, USA, 2007.
64. Marletta, G.; Iacona, F. Chemical and Physical Property Modifications Induced by Ion Irradiation in Polymers. In *Materials and Processes for Surface and Interface Engineering*; Springer: Dordrecht, The Netherlands, 1995; pp. 597–640.
65. Lewis, K.M.; Spazierer, D.; Urban, M.D.; Lin, L.; Redl, H.; Goppelt, A. Comparison of regenerated and non-regenerated oxidized cellulose hemostatic agents. *Eur. Sur.* **2013**, *45*, 2013–2020. [[CrossRef](#)]
66. Mengal, N.; Sahito, I.A.; Arbab, A.A.; Sun, K.C.; Qadir, M.B.; Memon, A.A.; Jeong, S.H. Fabrication of a flexible and conductive lyocell fabric decorated with graphene nanosheets as a stable electrode material. *Carbohydr. Polym.* **2016**, *152*, 19–25. [[CrossRef](#)]
67. Bodade, A.; Taiwade, M.; Chaudhari, G. Bioelectrode based chitosan-nano copper oxide for application to lipase biosensor. *J. Appl. Pharm. Res.* **2017**, *5*, 30–39.
68. Vidal, B.; Mello, M. Collagen type I amide I band infrared spectroscopy. *Micron* **2011**, *42*, 283–289. [[CrossRef](#)]
69. Martinez, G.; Millhauser, G. FTIR spectroscopy of alanine-based peptides: Assignment of the amide I' modes for random coil and helix. *J. Struct. Biol.* **1995**, *114*, 23–27. [[CrossRef](#)]
70. Meutter, J.; Goormaghtigh, E. Amino acid side chain contribution to protein FTIR spectra: Impact on secondary structure evaluation. *Eur. Biophys. J.* **2021**, *50*, 641–651. [[CrossRef](#)] [[PubMed](#)]
71. Vaideki, K.; Jayakumar, S.; Rajendran, R.; Thilagavathi, G. Investigation on the effect of RF air plasma and neem leaf extract treatment on the surface modification and antimicrobial activity of cotton fabric. *Appl. Surf. Sci.* **2008**, *254*, 2472–2478. [[CrossRef](#)]
72. Clougherty, L.; Sousa, J.; Wyman, G. Notes-C=N Stretching Frequency in Infrared Spectra of Aromatic Azomethines. *J. Org. Chem.* **1957**, *22*, 462. [[CrossRef](#)]
73. Tanvir, N.B.; Yurchenko, O.; Wilbertz, C.; Urban, G. Investigation of CO₂ reaction with copper oxide nanoparticles for room temperature gas sensing. *J. Mater. Chem. A* **2016**, *4*, 5294–5302. [[CrossRef](#)]
74. Nyquist, R.A.; Kagel, R.O. *Infrared Spectra of Inorganic Compounds*; Academic Press Inc.: New York, NY, USA; London, UK, 1971; p. 220.
75. Huang, C.; Chen, Y.; Liu, H. Characterization of Composite Nano-Bioscaffolds Based on Collagen and Supercritical Fluids-Assisted Decellularized Fibrous Extracellular Matrix. *Polymers* **2021**, *13*, 4326. [[CrossRef](#)]
76. Veleirinho, B.; Berti, F.V.; Dias, P.F.; Maraschin, M.; Ribeiro-do-Valle, R.M.; Lopes-da-Silva, J.A. Manipulation of chemical composition and architecture of non-biodegradable poly(ethylene terephthalate)/chitosan fibrous scaffolds and their effects on L929 cell behavior. *Mater. Sci. Eng. C* **2013**, *33*, 37–46. [[CrossRef](#)]
77. Jayakumar, R.; Nair, S.V.; Furuie, T.; Tamura, H. Perspectives of Chitin and Chitosan Nanofibrous Scaffolds in Tissue Engineering. In *Tissue Engineering*; InTechOpen: London, UK, 2010.
78. Rezaei, A.; Khanamani Falahati-Pour, S.; Mohammadzadeh, F.; Hajizadeh, M.R.; Mirzaei, M.R.; Khoshdel, A.; Fahmidehkar, M.A.; Mahmoodi, M. Effect of a Copper (II) Complex on The Induction of Apoptosis in Human Hepatocellular Carcinoma Cells. *Asian Pac. J. Cancer Prev.* **2018**, *19*, 2877–2884.
79. Bhavana, S.; Kusuma, C.G.; Gubbiveeranna, V.; Sumachirayu, C.K.; Ravikumar, H.; Nagaraju, S. Green route synthesis of copper oxide nanoparticles using Vitex altissima [L] leaves extract and their potential anticancer activity against A549 cell lines and its apoptosis induction. *Inorg. Nano-Met. Chem.* **2022**, *1*, 2470. [[CrossRef](#)]
80. Angelé-Martínez, C.; Ameer, F.S.; Raval, Y.S.; Huang, G.; Tzeng, T.J.; Anker, J.N.; Brumaghim, J.L. Polyphenol effects on CuO-nanoparticle-mediated DNA damage, reactive oxygen species generation, and fibroblast cell death. *Toxicol. Vitro.* **2022**, *78*, 105252. [[CrossRef](#)]
81. Liang, Y.; Chen, B.; Li, M.; He, J.; Yin, Z.; Guo, B. Injectable antimicrobial conductive hydrogels for wound disinfection and infectious wound healing. *Biomacromolecules* **2020**, *21*, 1841–1852. [[CrossRef](#)]
82. Hassan, M.A.; Omer, A.M.; Abbas, E.; Baset, W.M.A.; Tamer, T.M. Preparation, physicochemical characterization and antimicrobial activities of novel two phenolic chitosan Schiff base derivatives. *Sci. Rep.* **2018**, *8*, 11416. [[CrossRef](#)] [[PubMed](#)]
83. Fazal, A.; Ara, S.; Ishaq, M.T.; Sughra, K. Green Fabrication of Copper Oxide Nanoparticles: A Comparative Antibacterial Study against Gram-Positive and Gram-Negative Bacteria. *Arab. J. Sci. Eng.* **2022**, *47*, 523–533. [[CrossRef](#)]

-
84. Azam, A.; Ahmed, A.S.; Oves, M.; Khan, M.S.; Memic, A. Size-dependent antimicrobial properties of CuO nanoparticles against Gram-positive and -negative bacterial strains. *Int. J. Nanomed.* **2012**, *7*, 3527–3535. [[CrossRef](#)] [[PubMed](#)]
 85. Yang, J.H.C.; Teii, K.; Chang, C.C.; Matsumoto, S.; Rafailovich, M. Biocompatible Cubic Boron Nitride: A Noncytotoxic Ultrahard Material. *Adv. Funct. Mater.* **2020**, *31*, 2005066. [[CrossRef](#)]